


## SEQUENTIAL THERMAL ANALYSIS OF COMPLEX ORGANIC MIXTURES: PROCEDURAL STANDARDS AND IMPROVED CO<sub>2</sub> PURIFICATION CAPACITY

Ulrich M Hanke<sup>1,2\*</sup>  • Alan R Gagnon<sup>1</sup> • Christopher M Reddy<sup>2</sup> • Mary C Lardie Gaylord<sup>1</sup> • Anne J Cruz<sup>1</sup> • Valier Galy<sup>2</sup> • Roberta L Hansman<sup>1</sup> • Mark D Kurz<sup>1,2</sup>

<sup>1</sup>NOSAMS Laboratory, Geology and Geophysics, Woods Hole Oceanographic Institution, 266 Woods Hole Road, Woods Hole, MA, 02543 USA

<sup>2</sup>Marine Chemistry and Geochemistry, Woods Hole Oceanographic Institution, 266 Woods Hole Road, Woods Hole, MA, 02543 USA

**ABSTRACT.** Sequential thermal analysis allows for deconvoluting the refractory nature and complexity of carbon mixtures embedded in mineral matrices for subsequent offline stable carbon and radiocarbon (<sup>14</sup>C) isotope analyses. Originally developed to separate Holocene from more ancient sedimentary organic matter to improve dating of marine sediments, the Ramped Pyrolysis and Oxidation (RPO) apparatus, or informally, the “dirt burner” is now used to address pressing questions in the broad field of biogeochemistry. The growing interest in the community now necessitates improved handling and procedures for routine analyses of difficult sample types. Here we report on advances in CO<sub>2</sub> purification during sample processing, modifications to the instrumentation at the National Ocean Sciences Accelerator Mass Spectrometry (NOSAMS) facility, and introduce sodium bicarbonate procedural standards with differing natural abundance <sup>14</sup>C signatures for blank assessment. Measurements from different environmental samples are used to compare the procedure to the different generations of sequential thermal analyses. With this study, we aim to improve the standardization of the procedures and prepare this instrumentation for innovations in online stable carbon isotopes and direct AMS-interface measurements in the future.

**KEYWORDS:** chemical analysis, dirt burner, full oxidation (FOX) mode, radiocarbon dating, ramped pyrolysis oxidation.

### INTRODUCTION

Environmental carbon-bearing materials are inherently complex mixtures of inorganic and organic matter, often embedded in a mineral matrix (Hedges et al. 2000). The chemical compositions and isotopic signatures of the complex organic mixtures provide important means to elucidate origin, reactivity and age of carbon in environmental, archeological and geochemical research. An array of methods are employed to investigate the carbon isotopic composition in natural samples. Sequential thermal analysis is a powerful technique to characterize carbon mixtures and to target pools with similar bonding characteristics. The instrumentation (cf. Figure 1A) developed for this purpose at the National Ocean Sciences Accelerator Mass Spectrometry (NOSAMS) facility is a sequential thermal procedure, referred to as the Ramped Pyrolysis and Oxidation (RPO) apparatus or informally the “dirt burner” (Rosenheim et al. 2008). It has been used extensively for understanding the organic carbon provenance in natural (Rosenheim et al. 2008; Plante et al. 2013; Zhang et al. 2017; Zigah et al. 2017; Bao et al. 2018; Hemingway et al. 2018, 2019; Sanderman and Grandy 2020) and anthropogenic systems (Rogers et al. 2019). Several studies have investigated methodological aspects, instrumental performance, and sample pretreatment procedures (Fernandez et al. 2014; Hemingway et al. 2017a, 2017b; Bao et al. 2019).

The analytical approach was originally developed to separate Holocene from more ancient organic carbon in order to improve chronologies in Antarctic sediments (Rosenheim et al. 2008). Figure 1 illustrates the apparatus and analytical procedure. In brief, a sample is sequentially heated while carrier gas strips the evolved gases from a sample oven to a

\*Corresponding author. Email: [uhanke@whoi.edu](mailto:uhanke@whoi.edu)

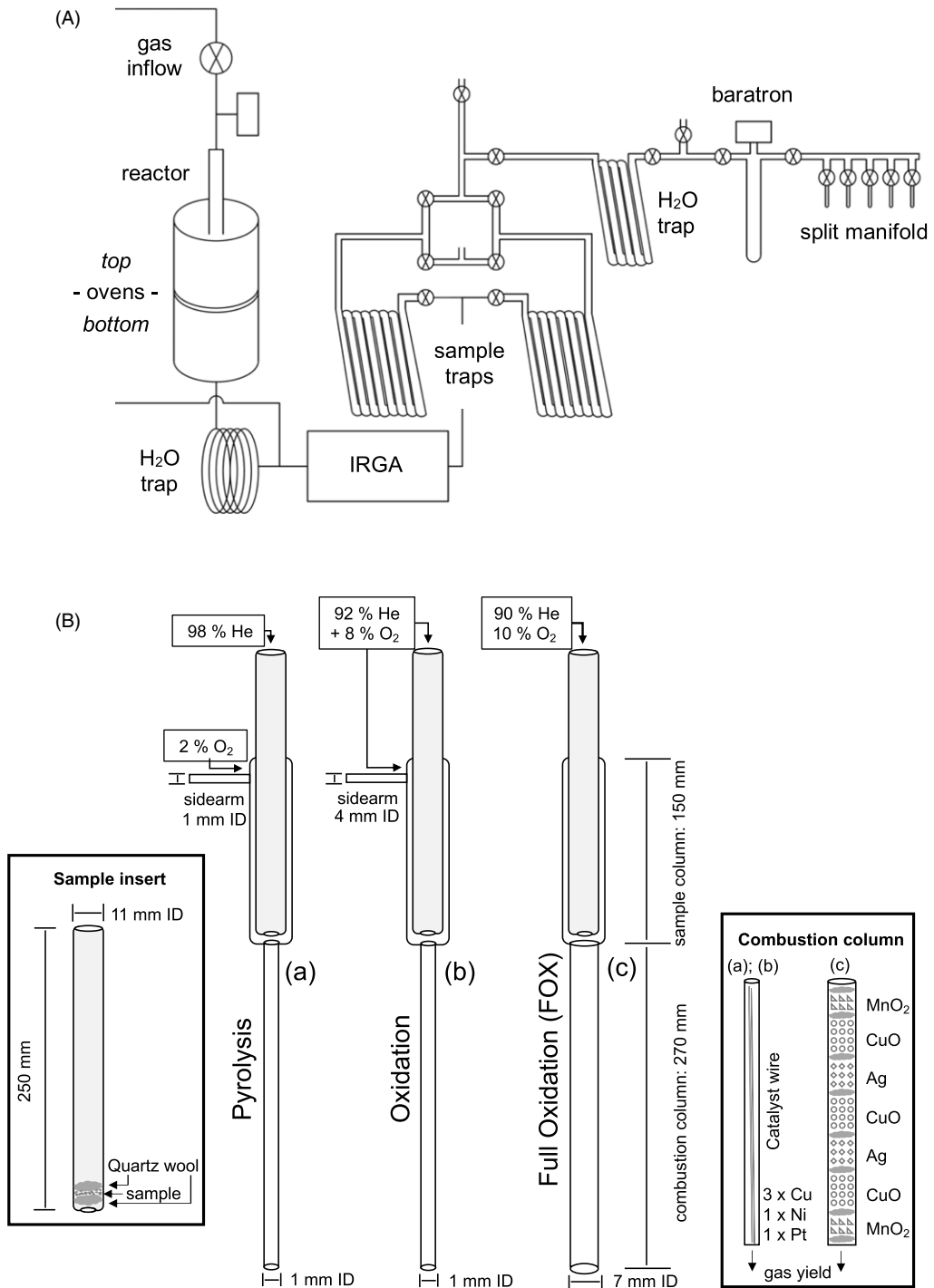


Figure 1 (A) Overview sketch of the NOSAMS RPO (aka "dirt burner") which includes the combustion columns (B) within the oven (reactor); (B) Overview of different combustion columns used in this study, including pyrolysis-RPO, oxidation-RPO and the full oxidation (FOX) mode described here (right inset). Note that the sidearm was used in (a) to supply the O<sub>2</sub> aside of the sample insert to oxidize thermally mobilized matter in the lower combustion section (800°C). In (b) it is available for switching between modes yet commonly is just flushed with premixed He + O<sub>2</sub> and thus was waived for (c) the full oxidation mode. During operation the entire combustion column is enclosed by the resistance furnace and operated between ambient temperature (25°C) and 1000°C.

combustion oven for oxidation, then through transfer lines into a flow-through cell equipped infrared-gas analyzer (IRGA), to glass coiled cryogenic sample collection traps for purification and isolation through a vacuum line for offline carbon isotope analyses.

In their initial work, Rosenheim et al. (2008) chose a pyrolysis quartz column (about 42 cm height) with helium as inert carrier gas transporting thermally released volatile carbon species from the sample-containing upper section (Figure 1B (a) upper section) to an oxidation zone in the bottom section that contains a catalyst wire, to which about 2% oxygen is supplied through a separate inlet (Figure 1B). As the system evolved, this setup was extended for usage in oxidation mode by using a 8% oxygen in helium mixture supplied throughout the entire system, resulting in the ramped pyrolysis-oxidation system that is in operation today at NOSAMS. The advantage of oxidation compared to the pyrolysis mode includes the minimization of artifacts from potential charring of biomass in the sample container (Figure 1B (b) upper section), and reducing the incomplete oxidation of released gases (Figure 1B (b) lower section) due to lack of the reagent oxygen. For samples releasing negligible quantities of interfering volatile species (chiefly sulfur and chlorine), e.g., for analysis of non-acid treated samples, pyrolysis and oxidation modes yield similar results (Grant et al. 2019; Hemingway et al. 2019). This system has proven versatile for a variety of applications and sample types, allowing for the isolation of CO<sub>2</sub> sample splits typically between 100 and 1000°C. It is routinely operated in either slow ramp (5°C min<sup>-1</sup>) to collect CO<sub>2</sub> fractions, or in fast ramp (20°C min<sup>-1</sup>) setting to define thermal behaviors. In the current user controlled setup, the CO<sub>2</sub> sample split size typically varies between about 30 µg C to several 100 µg C for offline analysis of stable carbon and natural abundance radiocarbon (<sup>14</sup>C) isotope composition. To purify the evolved gas, the current instrumentation comprises a custom-made catalyst wire: a braid of nickel, platinum, copper custom wires (1:1:3), as well as two water traps (propanol-filled dewars chilled with dry ice), one before the IRGA and one on the vacuum line.

However, the thermal heating of some environmental samples can result in the release of a mixture of volatile carbon and non-carbon molecules including chlorine and sulfur species. Depending on the amount of these impurities, they can precipitate on surfaces and compromise the reduction step when the CO<sub>2</sub> is graphitized for <sup>14</sup>C measurements. Therefore, sample recombustion with copper oxide wires (CuO) and silver (Ag) prior to graphitization is currently necessary to successfully produce filamentous carbon for AMS analyses and enhance gas purity for isotope ratio mass spectrometry. Eliminating the sample recombustion step would be beneficial for several reasons: First it would ease quality assurance by reducing the exposure of purified sample splits to potential extraneous carbon-bearing reagents; second it would reduce processing time and improve sample throughput. Finally, it could facilitate novel interface developments including an online (semi-)continuous stable carbon isotope analysis with cavity ring-down spectroscopy, the purification and loading of sample splits on molecular sieve cartridges or other sample transfer techniques for direct CO<sub>2</sub> <sup>14</sup>C measurement using a CO<sub>2</sub> gas ion source AMS, such as a MICADAS.

Previous research investigated the impact of different acidification procedures on the isotopic signatures of environmental sample materials and introduced a second packed combustion column (held at ~450°C) to enhance the gas purity, particularly for acid-fumigated samples (Bao et al. 2019). This served as a proof-of-concept that sequential thermal analyses with an additional oxidative combustion column yields comparable results. Nevertheless, these samples were recombusted with Ag and CuO and increased the length of transfer lines by

at least 1.5 m. A combination of the original RPO setup with the enhanced purification capacity of a packed chemical column with metal oxidant catalysts could simplify the analytical setup with improved gas purity. In this study we investigate the suitability of this column for gas purity, and if the recombustion step could be eliminated. Further we introduce a set of  $^{14}\text{C}_{\text{depleted}}$  and  $^{14}\text{C}_{\text{modern}}$  sodium bicarbonate procedural standards for quality control. We present data for a suite of typical materials including acid fumigated and high concentration sulfur samples that have been measured with the RPO/oxidation, and now with the novel full oxidation (FOX) mode combustion column, for comparison.

## MATERIALS AND METHODS

A suite of 7 samples including 2 pure chemicals, sodium bicarbonates ( $\text{NaHCO}_3$ ; CAS #: 144-55-8) as procedural standards, and 5 different environmental samples were used to test the full oxidation (FOX) column (Table 1). The actual matrix samples comprise a selection of different materials with varying carbon contents, spanning almost the entire range of natural abundance  $^{14}\text{C}$  signatures.

Briefly, the 5 samples include urban dust NIST SRM 1649a—a frequently studied environmental reference material (Currie et al. 2002)—collected in 1974 during the above-ground nuclear “bomb” testing period and thus perfectly suited to benchmark the new system. The Nantucket Mud Patch is an in-house NOSAMS ocean sediment standard material that is frequently used to test the performance of the RPO (Bao et al. 2019). The Gulf of Terror and Erebus Antarctic sediment (KC-5 24–25 cm) is the original sample material that was included in the first publication by Rosenheim et al. (2008) and is representative of samples with depleted  $^{14}\text{C}$  and low carbon contents. The other two samples constitute materials that are typical candidates of failure for the conventional combustion column setup because they require the recombustion of sample splits with Ag and CuO. These samples are the original acid fumigated Sierra Leone Rise sediment (Bao et al. 2019) and Wild Harbor Falmouth (USA) salt marsh sediment sample (36–39 cm), with high sulfur content (3.4% dry weight of acid rinsed sample).

The two  $\text{NaHCO}_3$  materials differ in their  $^{14}\text{C}$  content. The  $^{14}\text{C}$  depleted material was off-the-shelf (Matheson Coleman and Bell;  $\geq 99.7\%$  purity;  $F_m = 0.0119 \pm 0.0013$ ;  $\delta^{13}\text{C} = -5.7 \pm 0.4\%$ ;  $n = 5$ ) and the  $^{14}\text{C}$  modern material was produced at NOSAMS from the former by replacing the carbon signature with modern pure  $\text{CO}_2$  tank gas ( $F_m = 1.0398$ ; Airgas Inc.). In brief, 7.0 g of lab-grade  $\text{NaHCO}_3$  was dissolved in 100 mL high purity MilliQ water, placed on a stirring plate with bar and bubbled with tank  $\text{CO}_2$  gas for 30 min, then equilibrated for 12 hr under a 1 atm continuous flow  $\text{CO}_2$  gas stream and dried on a heating plate for 36 hr. The re-precipitated  $\text{NaHCO}_3$  was homogenized with mortar and pestle, transferred into a storage vial and dried at  $105^\circ\text{C}$  for 4 hr prior to storage in a desiccator to minimize absorbed water in the sample. The sample homogeneity was tested in repetitive ( $n = 6$ ) bulk carbon isotope measurements yielding a  $F_m = 1.0354 \pm 0.0021$  and  $\delta^{13}\text{C} = -4.2 \pm 0.1\%$ . The small variation of the  $^{14}\text{C}$  and stable carbon isotope compositions suggests that the newly produced  $\text{NaHCO}_3$  standard is homogenous.

### Full Oxidation (FOX) Mode

The setup of the RPO (sequential thermal) instrumentation at NOSAMS was described for pyrolysis mode (pyrolysis-RPO) in Rosenheim et al. (2008) and for the ramped pyrolysis oxidation mode (oxidation-RPO) in Hemingway et al. (2017a). The new column generation

Table 1 Sample details on types, pretreatment, and bulk carbon isotopic contents measured in this study or previously reported in the literature.

Sample name	Specifications	Pretreatment	C (%)	Bulk $^{14}\text{C}$ (Fm)	$\delta^{13}\text{C}$
Sodium Bicarbonate type 1	Pure compound	N/A	14.3 <sup>a)</sup>	$0.0119 \pm 0.0013$ <sup>a)</sup>	$-5.7$ <sup>a)</sup>
Sodium Bicarbonate type 2	Pure compound	N/A	14.3 <sup>a)</sup>	$1.0354 \pm 0.0021$ <sup>a)</sup>	$-4.2$ <sup>a)</sup>
NIST SRM1649a Urban Dust	Atmospheric particulates	N/A	17.7 <sup>b)</sup>	$0.5091 \pm 0.0020$ <sup>b)</sup>	$-25.2$ <sup>c)</sup>
Nantucket Mud Patch	Marine surface sediment	Acid-washed	1.2 <sup>c)</sup>	$0.8236 \pm 0.0039$ <sup>d)</sup>	$-19.6$ <sup>d)</sup>
Gulf of Terror and Erebus (KC-5 24-25 cm)	Antarctic marine core sediment	Acid-washed	0.4 <sup>d)</sup>	$0.0951 \pm 0.0025$ <sup>e)</sup>	$-25.4$ <sup>e)</sup>
Sierra Leone Rise	Carbonate-rich marine sediment	Acid-fumigated	0.7 <sup>c)</sup>	$0.1619 \pm 0.0012$ <sup>d)</sup>	$-17.6$ <sup>d)</sup>
Wild Harbor (091619-2 36–39 cm)	Sulfur-rich Salt marsh (3.4% S)	Acid-washed	14.2 <sup>a)</sup>	$0.9369 \pm 0.0019$ <sup>a)</sup>	$-17.9$ <sup>a)</sup>

<sup>a)</sup>this study; <sup>b)</sup>Hanke et al. (2017); <sup>c)</sup>NIST 1649a certificate of analyses; <sup>d)</sup>Bao et al. (2019); <sup>e)</sup>Rosenheim et al. (2008). Note the number of replicate analysis and measurement uncertainty ( $\delta^{13}\text{C}$ ) differs among the reported values from literature. Please refer to the original publications.

used in this study utilizes the same setup and specifications of the analytical protocol, but aims at enhancing the purification capacity and oxidation efficiency to yield high purity CO<sub>2</sub>. Therefore a custom-made column was acquired with a wider diameter bottom section (Figure 1B) than the pyrolysis column (widened from 1 to 7 mm ID) allowing to pack a granular combustion column with alternating layers of silver grains (99.99%; CAS: 7440-22-4; Alfa Aesar, manganese oxide powder ( $\geq 99\%$ ; CAS: 1313-13-9; Sigma-Aldrich) and CuO 4 × 0.5 mm wires ( $> 90\%$ ; CAS: 1317-38-0; Elemental Microanalysis).

In a first comparative experiment we interfaced the RPO with a residual gas analyzer (RGA) via open-split. In this experiment we aimed at tracing the purification capacity of oxidation-RPO and the novel FOX combustion column (see Appendix for details). Even though constraints on the experimental setup limited the information content, because the RGA compositional data are qualitative, the results indicated that the FOX column providing an enhanced CO<sub>2</sub> purification capacity.

The full oxidation (FOX) combustion column can be used within the existing instrumentation and thus allows to switch modes between the original pyrolysis, the oxidation and the novel FOX columns. In addition to the new column generation, the RPO system at NOSAMS was recently updated with digital flowmeters (Alicat Scientific, Tucson; model MC-50SCCM) in place of lower precision manual flowmeters, effectively increasing the accuracy of He carrier gas and O<sub>2</sub> supply to 0.01% of full scale reading. This allows better control of the carrier gas flow rate and ensures a constant proportion of 10% oxygen (instead of 8% used in earlier studies). The sidearm of the pyrolysis column used to supply oxygen in the original setting can be deactivated as it is superfluous in the oxidation mode, but poses a risk for memory effects between sample runs. Therefore, the sidearm was eliminated for the FOX mode column.

### Sample and Carbon Isotope Analysis

The analytical procedure in brief: the sample is weighed to target approximately 1 mg total C, transferred and packed between quartz wool in a quartz insert tube that is inset into the quartz reactor and sealed with ultratorr compression fittings. The system is purged with helium carrier gas and 10% O<sub>2</sub> at 35 mL min<sup>-1</sup> until CO<sub>2</sub> is stabilized at background values of  $0 \pm 5$  ppm, as measured using a CO<sub>2</sub> analyzer (Sable Systems International CA-10A). Only then the combustion oven was heated to 800°C and subsequently the sample oven was heated from room temperature to 100°C at 5°C min<sup>-1</sup> to start the sample heating. The isolation and purification of individual sample splits began at different time points and was continued until CO<sub>2</sub> evolution ceased and stabilized at less than 50 ppm. Note that thermograms, and thus total duration of analysis, including start and end temperature, vary with carbon composition and mineralogy of a respective sample.

The measurements were carried out in late March 2020. Glassware was freshly combusted 48 hr prior to use (reactor inserts at 800°C and sample storage tubes at 450°C both for 4 hr). The reactor was pre-baked at 800°C as well, then the custom column was packed and conditioned during two heating cycles (blank fast ramps) to minimize the impact of extraneous carbon from reagents before the start of the sample heating sequence. Twenty-seven samples were analyzed using the same FOX combustion column. Decisions on the isolation of individual sample splits were informed by online thermogram CO<sub>2</sub> evolution profiles aiming at (a) capturing periods of drastic variations, such as rise or depression of oxidized carbon, (b) plateaus that suggest

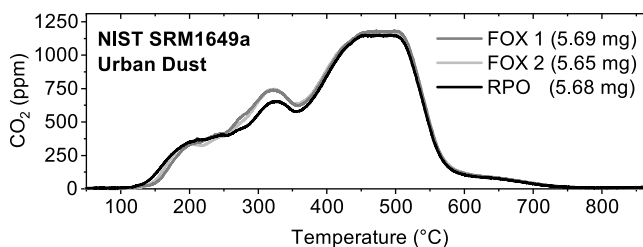


Figure 2 Comparison of CO<sub>2</sub> evolution profiles (thermograms) for NIST SRM1649a analyzed with the conventional RPO setup and the novel FOX combustion setup (in duplicate) at almost identical sample weight. Results support the similarity between RPO and FOX combustion reactors over the entire temperature range and highlight the slightly refined profile for FOX.

similar material composition, or (c) sample mass to yield similar split sizes in a sample. In contrast to the previous protocol, in this study the samples were processed without the additional combustion of the CO<sub>2</sub> splits with Ag and CuO, which previously was needed to purify the sample CO<sub>2</sub>. Instead, sample gas was directly expanded on the NOSAMS small sample line (SSL) vacuum system of which 96% of the gas was reduced to filamentous carbon (graphite) and 4% was used for IRMS <sup>13</sup>C measurements on a VG Prism-II or Optima system. Graphite targets were measured on the NOSAMS CFAMS system with a typical instrumental precision better than 3‰ and the CO<sub>2</sub> split for stable isotope composition on Prism/Optima with a typical IRMS precision of better than 0.2‰ (Xu et al. 2021).

### Data Processing

Information on the quantitative thermal evolution of CO<sub>2</sub> and on the respective combustion temperature for the samples were recorded in LabVIEW software through an infrared CO<sub>2</sub> analyser (IRGA; Sable Systems International CA-10A) and are illustrated in Figures 2 and 3. Regarding the isotope measurements, individual sample splits were stored in flame-sealed pyrex tubes for about four weeks before further analyses. Blank corrections of <sup>14</sup>C AMS data were carried out using the 96% mass yield through isotope mass balance calculations following the model of constant contamination published elsewhere (Hanke et al. 2017; Roberts et al. 2019). To explore whether this blank procedure can be implemented in routine application for a sequence of samples, we carried out single measurements for both bicarbonates and corrected the observed Fm to the accepted bulk value. Thereby we obtained two blank masses for <sup>14</sup>C depleted and modern contamination. Due to the lack of enough data to statistically derive the uncertainty, we assigned a 20% uncertainty to both mass and Fm and used this value to correct the individual splits of all five environmental samples.

For the first time, we used a set of NaHCO<sub>3</sub> procedural standards with <sup>14</sup>C<sub>modern</sub> and <sup>14</sup>C<sub>depleted</sub> signatures to determine a sequence-specific procedural blank value. The accurate blank determination in the sequential thermal decomposition of particulate carbon is inherently complex due to the steady temperature ramp from 100 to 1000°C at 5°C min<sup>-1</sup>. Here we test an indirect approach of a pure inorganic carbon material (sodium bicarbonate). Note that the “direct” and “indirect” blank determinations differ from one another. Whereas the



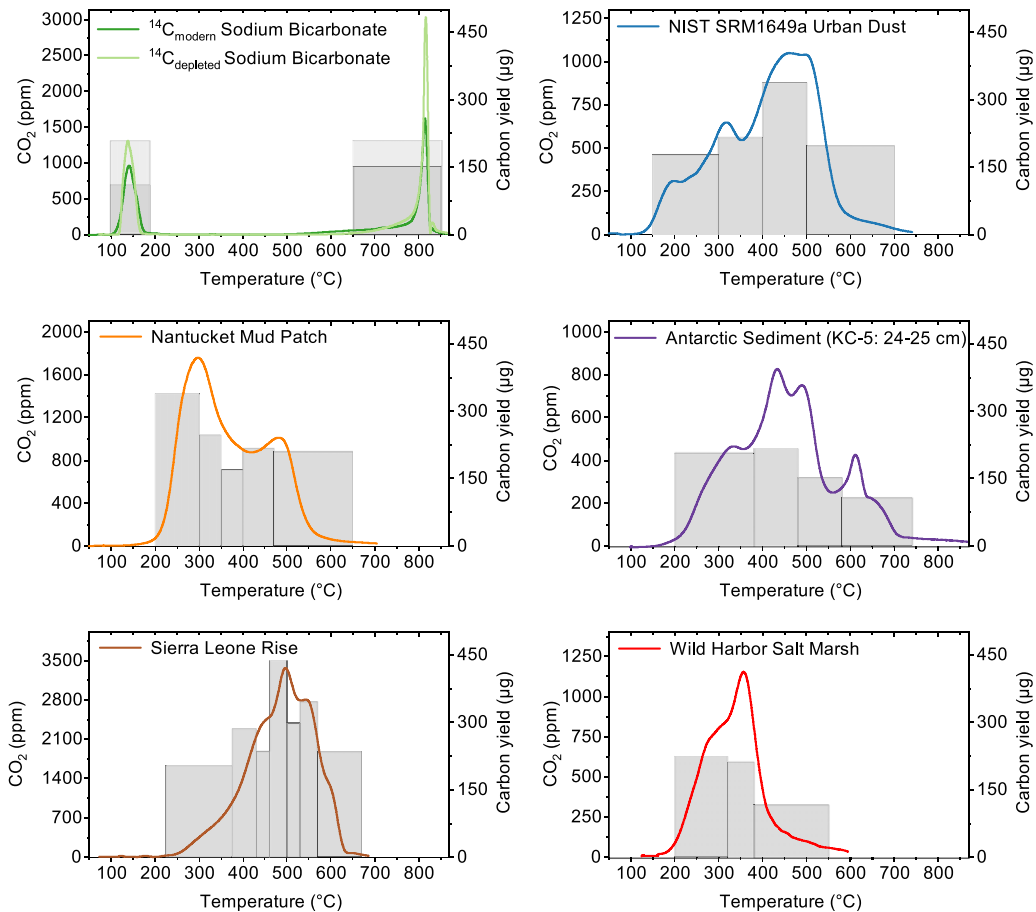


Figure 3 Sample thermograms showing CO<sub>2</sub> profiles (lines; ppm; left y-axis) for each sample with fraction yields (bar plots; µg C; right y-axis) over the identical temperature range. Sodium bicarbonate plot contains results for both materials, type 1 <sup>14</sup>C<sub>depleted</sub> (light green line and light gray bars) and type 2 <sup>14</sup>C<sub>modern</sub> (dark green line and dark gray bars).

“direct” method measures the carbon produced during a blank run without sample (using manometry), the “indirect” approach records the blank through the analysis of a well-characterized material, allowing assessment of the full procedural blank from calculation of the deviation from the accepted <sup>14</sup>C value (Xu et al. 2021). A previous study used CO<sub>2</sub> tank gas and found no indication of a shifting blank value or substantial isotopic fractionation during the ramping process (Hemingway et al. 2017a). With reference to this observation, the isolated splits for NaHCO<sub>3</sub> peak 1 (110–200°C) and peak 2 (650–850°C) were combined and compared to their bulk accepted Fm values. The resulting procedural blank was divided by the total duration of the collected fractions for sodium bicarbonates (290°C) to yield the total blank value per minute of fraction collection. Since almost all splits vary in the duration of fraction collection, this allows determination of the correct proportional blank per sample split and subsequently for the precise calculation of the actual blank-corrected sample <sup>14</sup>C values. Furthermore it comprises a procedural blank including loading of sample on the system, the sequential thermal analysis, the purification



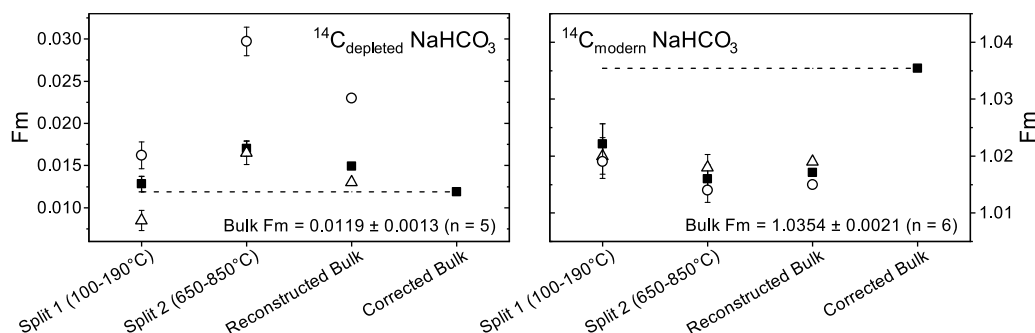


Figure 4 Details on individual  $^{14}\text{C}$  results ( $F_m$ ) from sodium bicarbonate splits (100–190°C and 650–850°C) with AMS uncertainty, mass-balance reconstructed bulk  $F_{m_{\text{measured}}}$  (only for sequence blank analysis illustrated in black squares) and bulk  $F_{m_{\text{corrected}}}$  after mass balance corrections with bulk  $F_m$  of accepted values (dashed lines). Independent blank analysis replicate 2 (open circles) and replicate 3 (open triangles) support the reproducibility of blank determinations using FOX combustion column with this set of sodium bicarbonates.

and isolation of  $\text{CO}_2$ , the blank of quartz tubes, and the SSL vacuum system blank with the additional uncertainty for the reproducibility in the AMS. To account for kinetic fractionation, the stable carbon isotope data were corrected following the procedure of Hemingway et al. (2017b).

## RESULTS AND DISCUSSION

A comparison between the novel FOX reactor and oxidation-RPO “dirt burner” analysis with NIST SRM1649a is shown in Figure 2. The temporal  $\text{CO}_2$  evolution profiles for subsequently isotopically resolved samples are illustrated in Figure 3. The  $^{14}\text{C}$  contents of individual and mass balance recombined  $\text{NaHCO}_3$  procedural standards are shown in Figure 4 and the  $^{14}\text{C}$  and  $\delta^{13}\text{C}$  data for the five typical environmental matrices are shown in Figure 5. Table 2 lists the temperature windows for all sample splits, with size, along with measured and corrected  $^{14}\text{C}$  data, including the results of the full error propagation versus AMS uncertainties.

In preparation to deconvolve the isotopic signatures of the five environmental samples with the novel FOX reactor, we compare the records on the thermal  $\text{CO}_2$  evolution with that of the conventional RPO. We selected the well-studied NIST SRM1649a Urban Dust for these analyses (Figure 2). To further evaluate the reproducibility of the analyses we measured duplicates for the FOX. The profiles show an overall similar thermal degradation pattern for both generations of combustion reactor. Despite the slightly earlier start of oxidation in the RPO (at about 125°C) and the slightly more pronounced  $\text{CO}_2$  maximum for the FOX analysis at about 320°C, the thermograms for both combustion generations evolve identically. The results provide confidence for the similarity of results for oxidation-RPO and FOX combustion reactors and set the stage for subsequent analyses.

### Temporal $\text{CO}_2$ Evolution Profiles

The main results (Figure 3) reveal different decomposition patterns for all sample types beginning around 100°C and effectively exhausted between 600 and 850°C. Only the inorganic procedural standards  $\text{NaHCO}_3$  show a baseline separation between peak 1 (100–190°C) and peak 2 (650–850°C). Measured  $\text{CO}_2$  maximum values range from 840 ppm in

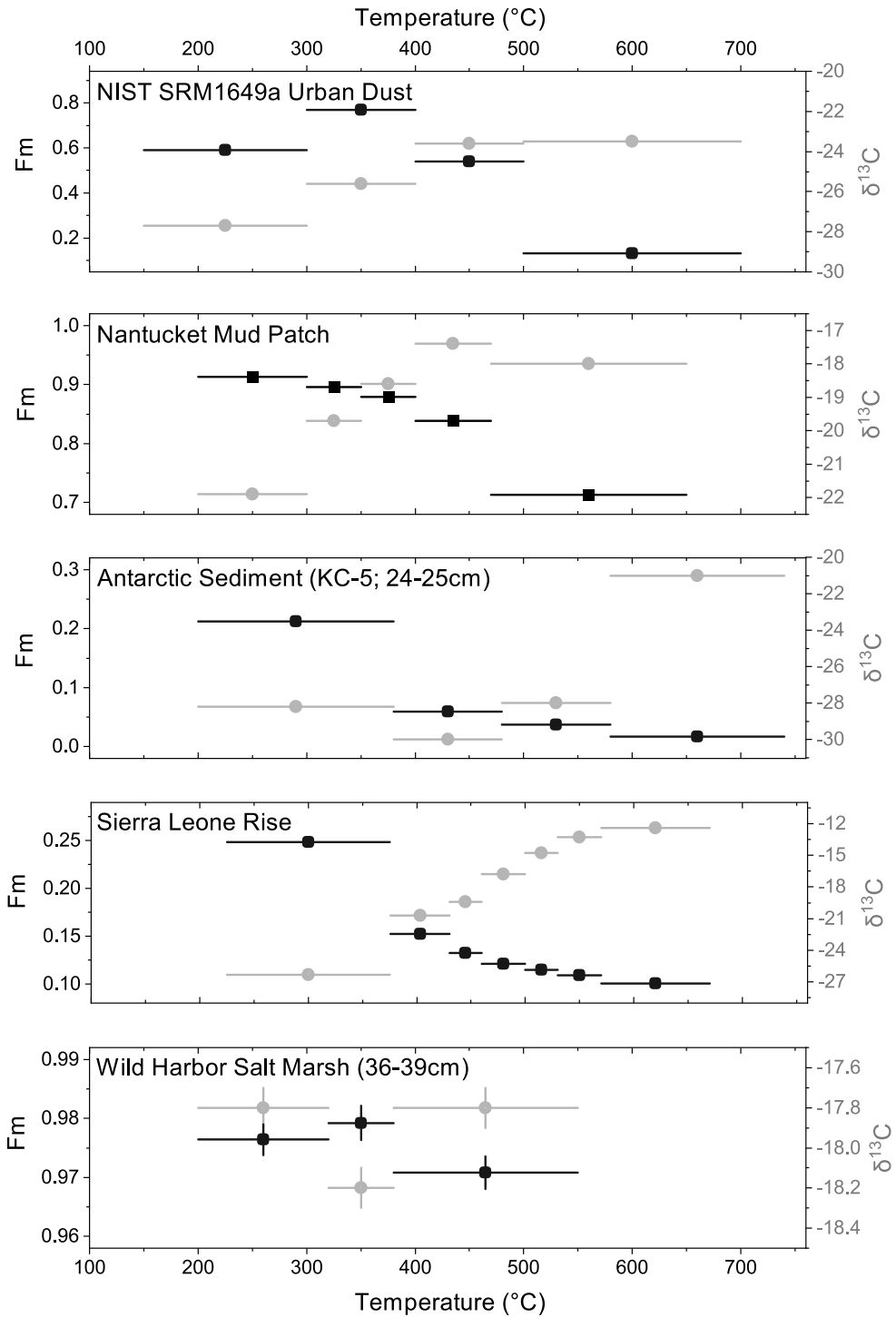


Figure 5 Results from carbon isotope analyses for samples showing  $Fm_{\text{corrected}}$  (black squares; left y-axis) and  $\delta^{13}\text{C}$  (gray circles; right y-axis). Note that dots mark mid-temperature of each split with horizontal lines indicating temperature range of each split. Vertical error bars show analytical uncertainties, but are generally smaller than the symbols, except for the Wild Harbor sample because of the similar isotopic signatures. Note that reported uncertainties are unusually small for these measurements—we determined a low-level blank mass and measured large sample masses.

Table 2 Sample splits and temperature range with mass,  $F_{m_{\text{measured}}}$  and  $F_{m_{\text{corrected}}}$  to illustrate the impact of mass balance blank correction for each sample as well as to show uncertainties from the AMS vs blank correction.

Sample	Split#	$\Delta\text{temp}$ (°C)	Mass ( $\mu\text{g C}$ )*	$F_{m_{\text{meas}}}$	$F_{m_{\text{sample}}}$	$F_m \Delta\% \text{ (meas - corr)}$	Total AMS uncertainty ( $\Delta\%$ )
NIST SRM1649a Urban Dust	1	150–300	161	$0.5846 \pm 0.0017$	$0.5894 \pm 0.0019$	-0.0048	0.221
	2	300–400	198	$0.7637 \pm 0.0018$	$0.7681 \pm 0.0019$	-0.0044	0.090
	3	400–500	305	$0.5388 \pm 0.0016$	$0.5403 \pm 0.0016$	-0.0015	0.040
	4	500–700	193	$0.1345 \pm 0.0010$	$0.1323 \pm 0.0013$	0.0022	0.343
Nantucket Mud Patch	1	200–300	289	$0.9096 \pm 0.0018$	$0.9135 \pm 0.0019$	-0.0039	0.050
	2	300–350	218	$0.8925 \pm 0.0020$	$0.8955 \pm 0.0020$	-0.0030	0.038
	3	350–400	156	$0.8747 \pm 0.0020$	$0.8788 \pm 0.0021$	-0.0041	0.065
	4	400–470	200	$0.8345 \pm 0.0019$	$0.8383 \pm 0.0020$	-0.0038	0.059
	5	470–650	206	$0.7067 \pm 0.0034$	$0.7128 \pm 0.0035$	-0.0061	0.124
Gulf of Terror and Erebus Antarctic Sed, KC-5 24–25 cm	1	200–380	181	$0.2129 \pm 0.0011$	$0.2120 \pm 0.0014$	0.0009	0.302
	2	380–480	222	$0.0612 \pm 0.0009$	$0.0596 \pm 0.0010$	0.0016	0.104
	3	480–580	150	$0.0394 \pm 0.0009$	$0.0367 \pm 0.0011$	0.0027	0.215
	4	580–740	105	$0.0234 \pm 0.0009$	$0.0173 \pm 0.0017$	0.0061	0.758
Sierra Leone Rise	1	225–375	176	$0.2485 \pm 0.0012$	$0.2482 \pm 0.0014$	0.0003	0.225
	2	375–430	231	$0.1529 \pm 0.0010$	$0.1523 \pm 0.0010$	0.0006	0.041
	3	430–460	197	$0.1327 \pm 0.0010$	$0.1322 \pm 0.0010$	0.0005	0.031
	4	460–500	350	$0.1213 \pm 0.0010$	$0.1209 \pm 0.0010$	0.0004	0.015
	5	500–530	242	$0.1154 \pm 0.0010$	$0.1149 \pm 0.0010$	0.0005	0.022
	6	530–570	284	$0.1097 \pm 0.0010$	$0.1092 \pm 0.0010$	0.0005	0.021
Wild Harbor Salt Marsh WH19 36–39 cm	7	570–670	211	$0.1017 \pm 0.0010$	$0.1003 \pm 0.0011$	0.0014	0.104
	1	200–320	197	$0.9692 \pm 0.0025$	$0.9764 \pm 0.0026$	-0.0072	0.109
	2	320–380	182	$0.9746 \pm 0.0028$	$0.9792 \pm 0.0029$	-0.0046	0.058
	3	380–550	113	$0.9539 \pm 0.0023$	$0.9708 \pm 0.0028$	-0.0169	0.535

\* $^{14}\text{C}$  split mass = total split–split for  $\delta^{13}\text{C}$  measurements. Mass was quantified on the NOSAMS small sample line.

the Antarctic sediment (Gulf of Terror and Erebus; KC-5 24–25 cm) to 3350 ppm in the Sierra Leone Rise sediment. All five environmental samples yielded distinct thermograms, indicating that they differ in their organic carbon composition and/or bonding characteristics. The bimodal to multimodal thermograms provide some insight into the heterogeneous nature of the organic matter, with thermochemically reactive fractions released at lower temperature.

The two distinct peaks at low and high temperatures for the bicarbonates in this study are almost identical to those reported by Rosenheim et al. (2008), in the premier publication on the RPO sequential thermal analysis in pyrolysis mode at NOSAMS. The good agreement between the two  $\text{NaHCO}_3$  thermograms (in light and dark green in Figure 3) demonstrates analytical reproducibility for the new column setup. The two different bicarbonates differ only in the magnitude of the  $\text{CO}_2$ , which may be due to higher carbonate purity in the off-the-shelf  $^{14}\text{C}_{\text{depleted}}$  material compared to the custom made  $^{14}\text{C}_{\text{modern}}$  standard. We suspect a higher amount of residual water in the latter standard, i.e., an incomplete drying process at  $105^\circ\text{C}$  for four hours prior to the analyses. However, the congruency of the two distinct peaks and the good agreement between the two thermograms suggests the absence of other impurities that could have caused the unequal yields using the same material mass.

The NIST urban dust 1649a sample reveals a broad thermogram with a wide maximum between  $450$  and  $500^\circ\text{C}$  preceded by a local maxima at lower temperatures, indicating a more refractory nature for the majority of carbon. This thermogram resembles the results of an evolved gas analyses (EGA) from the same standard reference material (Peralta et al. 2007) yet with visually more refined fluctuations in  $\text{CO}_2$  evolution resulting in a higher resolution thermogram. The apparent congruency between the thermogram of the RPO-FOX analytical setup and an EGA for the same material demonstrates the potential for the classification and comparison of known to unknown samples.

The NOSAMS in-house sediment standard Nantucket Mud Patch has a clear bimodal thermogram with a maximum at low temperature ( $300^\circ\text{C}$ ) which is indicative of a higher proportion of relatively thermochemically reactive carbon, and a distinct maximum at around  $500^\circ\text{C}$ . This sample has been analyzed to control the performance of the RPO instrument at NOSAMS and, for instance, was published by Bao et al. (2019) in a comparison of acidification pretreatment procedures. Our results indicate no substantial differences from their results using the oxidation-RPO combustion column.

In this study, the original Gulf of Terror and Erebus sediment sample (KC-5 34–35 cm) shows the most structure between  $200$  and  $740^\circ\text{C}$  with four maxima and a small shoulder at about  $650^\circ\text{C}$ . Even though seemingly in higher resolution, the thermogram with FOX here and pyrolysis mode (Rosenheim et al. 2008) show the same  $\text{CO}_2$  evolution with temperature increase. The first low temperature peak (around  $325^\circ\text{C}$ ) is apparent in both studies, which will be discussed in the isotope section below. We also find a sharp maximum at  $435^\circ\text{C}$  followed by a second at  $480^\circ\text{C}$  and another distinct peak at around  $615^\circ\text{C}$ . This indicates a diversity of substrate labilities and the presence of different organic matter types and perhaps differences in the provenance of organic carbon. This thermogram highlights the success of the original research to thermally deconvolve organic matter and thereby targeting individual fractions for discrete isotope analyses. It thereby unambiguously shows the abundant resolution with the full oxidation mode setup and suggests the absence of systematic differences between pyrolysis and FOX modes.

The Sierra Leone Rise sediment mineralizes between 220°C and 680°C with a distinct maximum at 500°C. This thermogram shows a small shoulder at 425°C and a minor second peak at 550°C following the maximum yet overall mimics a unimodal left-skewed distribution. With the apparent higher starting temperature this sample is composed of less volatile carbon compared to the others. A comparison of this thermogram with that reported by Bao et al. (2019) for the oxidation-RPO column shows some differences, for instance the location of the first shoulder differs by almost 100°C, and the absence of a second peak after the maximum. However, the starting and ending temperatures, and the location of the maximum at about 480°C, are identical and support the comparability of the two analytical procedures.

The Wild Harbor marsh sediment shows a narrow thermogram starting at about 160°C and decreases back to the instrumental background between 450 and 600°C (about 200 to <50 ppm). It appears with an almost unimodal thermogram distribution illustrated by a distinct peak at 350°C with a shoulder at about 280°C. Whereas this thermogram shape is typical for a marsh sediment, it showed an almost identical profile on the oxidation-RPO column (not shown, but similar to NIST SRM 1649a in Figure 2). This sample was used because of its high sulfur content (3.4%), which represents an extreme sample type that typically would necessitate an additional cleaning of CO<sub>2</sub> yields prior to isotope analyses.

### Indirect Blank Determination with NaHCO<sub>3</sub> Procedural Standards

The total indirect <sup>14</sup>C blank was determined using a set of bicarbonates (NaHCO<sub>3</sub>), the results of which are illustrated in Figure 4 including measured (split 1 and split 2), recombined and fitted (Fm-corrected) <sup>14</sup>C values for the <sup>14</sup>C<sub>modern</sub> and <sup>14</sup>C<sub>depleted</sub> end-members. These data comprise the upper and lower natural abundance <sup>14</sup>C signatures in typical environmental samples. While these procedural standards differ in their <sup>14</sup>C contents, both mineralize at the same temperature window and thus record the same experimental conditions. The carbon isotope content, however, is likely affected by partial release of CO<sub>2</sub> from the crystal lattice leaving behind sodium carbonate (Rosenheim et al. 2008). To reduce the complexity of this kinetic process, we mass-balance-corrected both peaks to yield a reconstructed bulk value that records the <sup>14</sup>C<sub>modern</sub> and <sup>14</sup>C<sub>depleted</sub> blank (Figure 4; solid squares) over a total duration of 290°C which is equal to a duration of 58 minutes. The difference of the reconstructed to the accepted values account for 3 per mil for the <sup>14</sup>C<sub>depleted</sub> and 18 per mil in the <sup>14</sup>C<sub>modern</sub> sample. The combination of both blank values result in a total blank of Fm = 0.268 ± 0.054 and a blank mass of 4.4 ± 0.9 µg C for the same time period and ΔT. Included in the total blank is the small sample line blank, which is 0.35 µg C, and is minor (within uncertainty), yielding a total sequence blank value of 0.069 µg C min<sup>-1</sup> (13.8 ng C °C<sup>-1</sup>) during discrete sampling with the FOX column. This calculation of a universal blank is possible because of the absence of a systematic or sudden shift caused by isotope fractionation processes in the sequential thermal analyses (Hemingway et al. 2017a).

This indirect blank assessment for the FOX column reveals a total blank of only about 34% compared to the first comprehensive blank assessment of the RPO (Fernandez et al. 2014). More recent assessments in that laboratory yielded lesser total blank levels of 2.8 and 3.7 µg C, respectively (Subt et al. 2017; Venturelli et al. 2020). Both studies utilized the oxidation-RPO. The results indicate that blank levels—via the indirect assessment using external standard materials—are similar for both combustion columns.

In comparison to blank data determined with the direct blank approach, toggling sample traps in the oxidation-RPO (Hemingway et al. 2017a) at NOSAMS, the results of this study are higher (about  $9.4 \text{ ng C } ^\circ\text{C}^{-1}$ ). This difference between the direct and indirect assessment has been observed in other studies, for instance by Xu et al. (2021), and is likely due to the fundamentally different experimental approaches. The direct system blank reflects specific aspects of the instrumental setup up to measurement of carbon abundances. The indirect blank determinations, with procedural standards, includes all sample processing steps, and thus are more representative of the actual analyses of environmental sample matrices. Nonetheless the good agreement of the systematic direct characterization by Hemingway et al. (2017a) with our results supports the indirect blank procedure using  $\text{NaHCO}_3$  as procedural standards and suggest that the “dirt burner” overall yields similar blanks for the oxidation-RPO and the FOX-RPO combustion column discussed here.

The use of external standards entails information about the  $^{14}\text{C}$  signature in addition to the total blank level and thus provides insights on the composition of blank (Santos et al. 2007). Sources of blanks are presumed to originate from at least ambient air, potential impurities of gases and residuals of organic solvents used for cleaning the instrument. Seasonal outside conditions such as fossil fuel burning nearby as well as vegetation productivity can influence the  $^{14}\text{C}$  composition through lab air intakes and thus impact the ambient air  $^{14}\text{C}$  signature among geographic locations of laboratories. The use of dry ice can also potentially impact the  $^{14}\text{C}$  signature of lab air. Nonetheless procedural blanks may change over time due to evolving instrumental performance between maintenance intervals and individual operators.

In an effort to ensure that the sequence blank is robust, we carried out additional analyses on the bicarbonates, with a freshly packed FOX reactor. The results are plotted as open symbols (Figure 4) to show the overall similarity between the blank values used to correct the environmental samples in this study. The calculated blank mass for the three reconstructed bulk  $^{14}\text{C}_{\text{depleted}}$   $\text{NaHCO}_3$  analyses varied between 0.23 and  $4.80 \mu\text{g C}$  and for  $^{14}\text{C}_{\text{modern}}$  between 3.1 and  $5.9 \mu\text{g C}$ . With reference to the two-endmember blank assessment, we observe a larger variability in  $^{14}\text{C}_{\text{depleted}}$  bicarbonates (Figure 4 left panel) particularly in the high temperature split than we observe for the modern counterpart. The correction of thermally deconvolved bicarbonates with bulk Fm values, however, enable to correct for the overall blank level and its magnitude also serves as an indicator for the robustness of analytical setup during a sequence of sample analyses.

Based on correction of the bicarbonate measurements, shown in Figure 4, the blank level is about  $1.4 \mu\text{g C}$  for the collection of a sample split over a temperature range of  $100^\circ\text{C}$  (heating rate:  $5^\circ\text{C min}^{-1}$ ). This blank mass is similar to other molecular-level  $^{14}\text{C}$  analyses (Santos et al. 2010; Hanke et al. 2017; Haghypour et al. 2019) and lower than bulk  $^{14}\text{C}$ -DOC analyses (Xu et al. 2021). Further, a normalization of our sample splits (Table 2) to a theoretical split size of  $100^\circ\text{C}$  for all samples in this study, shows split sizes of 68–912  $\mu\text{g C}$  (the disparity is caused by the dynamic evolution of thermograms), which translates to blank mass contributions of only 0.17–2.05% per split. In other molecular-level  $^{14}\text{C}$  analyses, this relationship can exceed 10% (Hanke et al. 2017), depending upon sample type and sample size. This relationship of blank and sample mass provides some indication for the overall precision of sample data after the mass-balance corrections illustrated in Table 2.

To correct sample data, the blank  $^{14}\text{C}$  signature is equally important to mass. We determined the  $^{14}\text{C}$  signature of the blank to be  $F_m = 0.268 \pm 0.054$ . This agrees well with the average blank ( $F_m = 0.314$ ) reported by Fernandez et al. (2014). In contrast, Hemingway et al. (2017a) found a higher blank  $^{14}\text{C}$  signature ( $F_m = 0.555 \pm 0.042$ ), indicating a lesser contribution of  $^{14}\text{C}_{\text{depleted}}$  sources such as petroleum-derived solvents. We showed that this set of  $^{14}\text{C}_{\text{modern}}$  and  $^{14}\text{C}_{\text{depleted}}$   $\text{NaHCO}_3$  are suitable procedural standards to trace the blank level in sequential thermal  $^{14}\text{C}$  analyses, allowing each operator to control their own batch blank values. A careful blank procedure is particularly important as the combination of packing new columns, maintenance intervals, marginal differences in handling the instrument, and also storage of standard materials, can alter blank values. This should be taken into consideration for yielding good quality data, i.e., that allow for reproducible analysis and robust interpretation of data. An indirect blank assessment can provide sufficient data to assign an average blank value and to document robust differences in blanks for the different types of combustion columns. As an outlook towards online  $\delta^{13}\text{C}$  analysis it may become useful to supplement the set of bicarbonates standards for  $^{14}\text{C}$  with some mid-T-coals with largely differing  $^{13}\text{C}$  contents. As a counterpart to the inorganic materials this would be helpful for high precision analysis of pure materials that mineralize at intermediate temperatures.

### Deconvoluted Sample Isotopic Signatures

Sequential thermal analyses provide the opportunity of resolving bulk materials into discrete fractions and are useful for identifying target fractions for  $^{14}\text{C}$  dating, determining autochthonous/allochthonous organic matter sources, tracing impact of anthropogenic carbons, or disentangling short versus long term carbon cycles. The focus here is primarily on the dynamic range of  $^{14}\text{C}$  in a sample, along with the natural abundance spectrum, to illustrate both potential and performance. The temperature range for each sample split with carbon yield is included in Figure 3 and the isotope data are illustrated in Figure 5.

The isotope data reveal a dynamic behaviour for both  $^{14}\text{C}$  and  $\delta^{13}\text{C}$ , with higher  $\delta^{13}\text{C}$  signatures associated with lesser  $^{14}\text{C}$  contents (Figure 5). For  $^{14}\text{C}$ , the samples span a large range of natural abundance  $^{14}\text{C}$ , from  $F_m = 0.109$  in the Sierra Leone high temperature split to  $F_m = 0.979$  in the mid-temperature Wild Harbor Marsh sediment sample. This implies that any distinct signature of the above-ground nuclear bomb testing is absent in these samples, or at least muted due to dilution with more  $^{14}\text{C}$ -depleted materials. The  $\delta^{13}\text{C}$  values vary from  $-30.0\text{‰}$  intermediate temperature (split 2) Antarctic sediment to  $-12.4\text{‰}$  in the high temperature (split 7) Sierra Leone Rise sediment, suggesting large differences in organic matter provenance. We observe smaller  $\delta^{13}\text{C}$  variability in the Nantucket Mud Patch, Antarctic sediment and Wild Harbor Marsh sediment (Figure 5; y-axis scales), which is consistent with the  $^{14}\text{C}$  values. In contrast we found the largest sample heterogeneity in the NIST 1649a Urban Dust sample with differences between fractions ( $\Delta F_m$ ) of up to 0.635  $F_m$ . The Urban Dust and Marsh sediment both reveal higher  $^{14}\text{C}$  contents in the second split compared to the first split, whereas the other three samples show decreasing  $^{14}\text{C}$  contents with increasing temperature. This indicates that low temperature (more thermochemically reactive) organic matter seems to consist of a larger portion of contemporary carbon and the portion of “older” (comparatively  $^{14}\text{C}$ -depleted) more refractory carbon increasingly dominates the higher temperature splits. These systematic trends support the potential of resolving the organic matter complexity via carbon isotope signatures through sequential thermal analyses.



NIST 1649a Urban Dust was sampled in four fractions revealing heterogeneous  $^{14}\text{C}$  distributions with  $F_m = 0.132$  (split 4) to  $F_m = 0.768$  (split 2) yet with a lesser dynamic range in  $\delta^{13}\text{C}$  ( $-23.5$  to  $-27.7\%$ ). The latter follows a clear trend of increasing  $^{13}\text{C}$  depletion with higher temperature whereas the  $^{14}\text{C}$  increases from split 1 to split 2 and stepwise shows quite depleted  $^{14}\text{C}$  values, pointing towards dominating  $^{14}\text{C}_{\text{depleted}}$  carbon sources. As this reference material originates from an almost annual sampling of ambient air in a public parking garage (NIST, 2007), the impact of residues from incomplete combustion of engine fuels is assumed (Currie et al. 2002). A comparison to literature values for high temperature split 4 shows similarities between results of black carbon analyses, for instance for bulk chemical oxidation/residue of elemental carbon ( $F_m = 0.17$ ) or targeted aromatic carbon (CuO oxidation after methylene chlorine extraction) analyses ( $F_m = 0.153$ ). Both are included in a large interlaboratory comparison by Currie et al. (2002). A molecular-level study, using the source-specific black carbon markers benzene polycarboxylic acids (BPCAs), yielded a  $^{14}\text{C}$  signature of  $F_m = 0.088$  (Hanke et al. 2017). Another study focused on the biogenic contribution to the solvent-extracted unresolved complex mixture (UCM), as well as to three fractions of *n*-alkanes ( $n\text{C}_{20}\text{-}n\text{C}_{22}$ ;  $n\text{C}_{24}\text{-}n\text{C}_{26}$ ;  $n\text{C}_{28}\text{-}n\text{C}_{30}$ ), and found an almost fossil  $^{14}\text{C}$  signature ( $F_m = 0.007\text{--}0.029$ ) (White et al. 2013). Both specific molecular-level studies reported lesser  $^{14}\text{C}$  contents than split 4 ( $500\text{--}700^\circ\text{C}$ ;  $F_m = 0.132$ ) in this study. The high-temperature split is more  $^{14}\text{C}$  depleted than the operationally defined bulk aromatic black carbon data (Currie et al. 2002). We infer that this high-temperature fraction records combustion and petroleum products of similar bonding energies. Apart from its predominance in fossil fuel residuals, the carbon isotope composition for this sample has not been previously characterized. Nevertheless, this material appears to be well suited to be used in benchmark analyses for similar instrumentation in future research.

The Nantucket Mud Patch reveals decreasing  $^{14}\text{C}$  values with increasing temperature from split 1 to split 5 ( $F_m = 0.914$  and  $F_m = 0.713$ , respectively). In contrast, the  $\delta^{13}\text{C}$  values rise ( $-21.9$  to  $-17.4\%$ ) between split 1 and split 4 and reveal a slightly lower  $\delta^{13}\text{C} = -18\%$  for split 5. An interpretation of the latter is limited due to a potential isotope fractionation that might compromise interpretations of  $\Delta\delta^{13}\text{C} \leq 2\%$  (Hemingway et al. 2017a; determined on the oxidation-RPO combustion column). This in-house sediment standard was also studied by Bao et al. (2019) in a study to investigate the impact of acid pretreatment procedures for oxidation-RPO analysis. They isolated fractions of slightly different temperature windows, but the overall trends are consistent, with decreasing  $^{14}\text{C}$  signatures at increasing temperature. However, while the  $^{14}\text{C}$  contents are very similar in split 1 ( $\Delta F_m = 0.009$ ), they differ in the high-temperature split with  $\Delta F_m = 0.396$ . The latter quite likely is due to the longer duration of purification and different temperature windows of collection in the two studies. Indeed, considering the  $^{14}\text{C}$  depletion trend observed with increasing temperature and the lack of evidence for isotope homogeneity among individual temperature splits, it is not surprising that our high-temperature split ( $500\text{--}600^\circ\text{C}$ ) is less  $^{14}\text{C}$  depleted than reported by Bao and collaborators ( $558\text{--}900^\circ\text{C}$ ) because the latter integrates over a more refractory section of the reactivity continuum. We chose to stop the analyses when the online  $\text{CO}_2$  measurement decreased monotonously to less than 50 ppm  $\text{CO}_2$  due to constraints in the instrumental precision of the  $\text{CO}_2$  analyser (10% of reading plus drift) to ensure some robust signal-to-noise ratios. This limits the comparability of the results but also illustrates the potential for additional measures, such as online monitoring of stable isotope composition that could assist in the identification of changes in substrate composition. Nonetheless, in the comparison between the isotope values of

oxidation-RPO-equipped chemical oven with that of FOX for this sample, we clearly see the same trends with temperature evolution, with different resolution.

The Antarctic sediment reveals a clear trend along four splits towards more depleted  $^{14}\text{C}$  signatures ( $F_m = 0.212\text{--}0.017$ ) with an abrupt change between split 1 and split 2 ( $\Delta F_m = 0.152$ ). In contrast,  $\delta^{13}\text{C}$  again show an opposing trend with  $-28.2$  to  $-21.0\text{‰}$  with an additional  $-1.8\text{‰}$  depression in split 2. This sample was first described by Rosenheim et al. (2008) when they reported the first NOSAMS carbon isotope data in pyrolysis mode. The aim of their study was to isolate autochthonous organic carbon that would facilitate  $^{14}\text{C}$  dating of Antarctic sub-ice shelf sediment. Focusing on sediments from two locations, their results from site K-49 demonstrated the successful application of this novel instrumentation. For the other site (Gulf of Terror and Erebus; KC-5 24–25 cm) in this study, they measured a low and high temperature split and observed more  $^{14}\text{C}$ -depleted carbon in the lower temperature split that were inconsistent with results on co-deposited foraminifera. In contrast, we obtained about 11200  $^{14}\text{C}$  years (split 1) which is approximately 5300  $^{14}\text{C}$  years younger than previously reported (Rosenheim et al. 2008) and, with reference to the foram-based sediment chronology, it likely reflects the correct age of sediment burial at this location. These results demonstrate an adequate analytical resolution that matches the initial pyrolysis-RPO and provide an analytical capacity to develop sediment chronologies even in extreme environments with minor autochthonous inputs.

Among the two samples with high levels of chlorine and sulfur, we analyzed the acid-fumigated Sierra Leone Rise sediment in seven sample splits. Results show decreasing  $^{14}\text{C}$  contents ( $F_m = 0.248\text{--}0.100$ ) between split 1 and split 7 with an initial drop between split 1 and split 2 ( $\Delta F_m = 0.096$ ). In this sample set we detected the largest  $\delta^{13}\text{C}$  range, from  $\delta^{13}\text{C} = -26.3$  to  $-12.4\text{‰}$  with a  $5.6\text{‰}$  difference between split 1 and split 2. Thus the more refractory carbon contains a heavier isotope signature. We used the acid-fumed bulk  $\delta^{13}\text{C}$  value reported by Bao et al. (2019) as a reference to correct the measured data and yielded a mass balance-corrected  $\delta^{13}\text{C} = -17.2\text{‰}$ , which differs only by  $0.4\text{‰}$  from the reported bulk value. In agreement with the other samples, the post-blank corrected values represent typical  $\delta^{13}\text{C}$  signatures for organic carbon in sediments and record a  $^{13}\text{C}$  depletion between thermochemically reactive and more refractory carbon.

The Wild Harbor Marsh sediment (WH 36–39 cm) serves as a test sample with high sulfur content (3.4%). Results for three sample splits show a relatively homogenous composition for both  $^{14}\text{C}$  ( $F_m = 0.979\text{--}0.971$ ) and  $\delta^{13}\text{C}$  ( $-18.2$  to  $-17.8\text{‰}$ ). Similar to the other samples, we observe slightly higher  $^{14}\text{C}$ ; the  $\delta^{13}\text{C}$  signature remains steady, but is lower in split 2 compared to the other splits. The differences are small ( $\Delta F_m = 8\text{‰}$  and  $\Delta\delta^{13}\text{C} = 0.4\text{‰}$ ) and might reflect analytical uncertainties. Previous research determined the sediment accumulation rate at this location at  $0.35\text{ cm yr}^{-1}$ , derived from constant initial concentration model with  $^{210}\text{Pb}$  and  $^{137}\text{Cs}$  yielding an age of deposition of about 105 years BP at this depth (White et al. 2005). Another study reported congruent down-core  $^{14}\text{C}$  contents for the microbial community (phospholipid fatty acids) and TOC at this location (Slater et al. 2005). It suggests that the microbial consumption of autochthonous sedimentary organic matter similarly affects the full organic matter spectrum (thermochemically reactive to refractory). Thus the absence of preferential degradation and decomposition in this sample that was buried by tidal and Marsh debris about 100 years ago can explain the minor isotopic variations in the three sample splits.

In summary, there was no indication of impurities within the CO<sub>2</sub> fractions generated with the FOX combustion column during production of filamentous carbon or IRMS analyses in any of the samples. Using the RPO/FOX procedure all of the samples were successfully processed ( $n = 27$ ) and analyzed for <sup>14</sup>C and δ<sup>13</sup>C, including the two samples with high levels of chlorine and sulfur. This suggests the effective purification capacity of the FOX combustion column, and that the previously required recombustion with Ag and CuO is no longer necessary. Therefore, the procedure allows for faster sample throughput without additional chemicals that would add to the blank. It also facilitates direct sealed-tube graphitization or potentially online isotope monitoring, with lesser risk of secondary gases that can compromise instrumentation and might have corrosive effects in transfer lines and detectors.

### Impact of Blank Correction and Precision of Data

The results of <sup>14</sup>C measured versus corrected data for the five environmental samples (splits:  $n = 23$ ) are illustrated in Table 2 using the sequence blank ( $13.8 \pm 2.8 \text{ ng C } ^\circ\text{C}^{-1}$  and  $F_m = 0.268 \pm 0.054$ ). Note that the <sup>14</sup>C contents of samples vary between  $F_m = 0.017$  and  $0.979$  and thus span almost the full spectrum of natural <sup>14</sup>C abundances. Because of the depleted blank <sup>14</sup>C signature the impact of correction will be largest for modern samples compared to samples with lower <sup>14</sup>C content with less effect on the precision. The magnitude of blank corrections ranges from  $-16.9\%$  (split 3; Wild Harbor Marsh) to  $+6.1\%$  (split 4; Antarctic Sediment). Even though minor, this is a substantial change of sample  $F_m$  if compared to the surprisingly small change in uncertainties (total uncertainties-AMS) up to  $0.8\%$ . This very minor increase in the overall uncertainties of measurement after the error propagation demonstrates overall the robust approach for molecular-level <sup>14</sup>C analyses. Considering the variabilities and potential inaccuracies that may be expected from multistep procedures, the correction of data appears mandatory even though the impact overall remains small for the comparatively large sample mass compared to isotope analysis of molecular markers (Santos et al. 2010).

Mass balance calculations of blank corrections impacted the splits among a sample more than between different samples. In this study the average duration of each split is 20 min or 100°C (between 30 and 200°C). With this variability in split duration, we determined an average split size of  $207 \pm 58 \text{ } \mu\text{g C}$  (between 113 and 350  $\mu\text{g C}$ ). With respect to the dynamic nature of thermogram evolution for different sample types and the variability in <sup>14</sup>C contents, this result may reflect a typical scattering in fraction size where individual split sizes sometimes even account for much less with only 50  $\mu\text{g C}$ . The thermal heating gradient of a sample typically results in differing <sup>14</sup>C signatures for the individual splits. Here the blank correction of data for split sizes and sampling duration allows determination of the actual isotopic composition of discrete fractions in a sample.

A correction of sample data with procedural standards is most precise if sample <sup>14</sup>C falls within the modern and depleted <sup>14</sup>C signatures. In this study we used a set of <sup>14</sup>C<sub>modern</sub> ( $F_m = 1.0354 \pm 0.0021$ ;  $n = 6$ ) and <sup>14</sup>C<sub>depleted</sub> ( $F_m = 0.0119 \pm 0.0013$ ;  $n = 5$ ) pure NaHCO<sub>3</sub> procedural standards to access the magnitude of the blank including the associated uncertainty and to correct the data. Yet, a NaHCO<sub>3</sub> standard with custom <sup>14</sup>C contents spanning a larger <sup>14</sup>C range could easily be produced at a similar high precision.

### **Potential of Full Oxidation Mode Columns for Interface Development**

The successful installation of the RPO sequential thermal analysis instrumentation at NOSAMS over a decade ago has been extensively used to understand organic matter complexity. It has substantially improved our understanding of the global carbon cycle, including the identification of adequate autochthonous organic carbon for  $^{14}\text{C}$  dating, the fate of carbon across landscapes, and its powerful application in environmental forensics. To further advance the applicability and to expand the results with additional information, the incorporation of online  $\delta^{13}\text{C}$  monitoring as well as routine quality assurance procedures would result in improved precision and accuracy.

As discussed in this paper, the interpretation of distinct thermograms bear uncertainties for the identification of specific substrate types. A proof of concept study investigated the use of cavity ring-down spectroscopy to monitor discrete fractions of evolved  $\text{CO}_2$  yields (Cruz et al. 2017) during the sequential thermal analysis. The instrument failed to operate after the initial measurements, which may have been caused by corrosion of the detector by secondary gas species that were incompletely removed. Although this is not definitive, there are several lines of evidence that the custom-made wires used in the pyrolysis-RPO and oxidation-RPO setups incompletely purified the evolved  $\text{CO}_2$ , resulting in the presence of oxidative nitrogen-, chlorine-, and sulfur-species. This eventually necessitated the sealed-tube combustion with  $\text{CuO}$  and  $\text{Ag}$  to successfully form filamentous carbon or measure the stable C isotopic composition on the IRMS. With the novel FOX combustion column, this extra step will no longer be necessary.

The good agreement between thermogram shape and isotope data between the pyrolysis/oxidation combustion columns and the novel FOX mode suggests no constraints for alternating use. With the FOX combustion column for the NOSAMS setup, we obtained successful analyses even for extreme types of organic mixtures in environmental samples without recombustion. The improved gas purification may now allow for online isotope monitoring with lesser risk to corrode the instrumentation. Further, it can also allow for sealed-tube zinc graphitization, a procedure that has recently been reported to return precise AMS data even for microscale sample amounts (Walker and Xu 2019). This is a powerful sample processing procedure as it would allow to process splits (roughly 4–5 splits per sample) of two to three samples a day, graphitize overnight and have filamentous carbon ready for AMS analyses the next morning. Alternatively, the reduced carbon produced in sealed glass tubes can be stored for years without affecting the quality of the material. This largely increases sample throughput and accompanied by some procedural blanks it enables quality assessment for the operator while reducing labor costs for additional sample processing. Further developments in the future might also comprise the design of a sequential thermal analyses setup with multiple combustion columns that automatically transfer  $\text{CO}_2$  splits on molecular sieve traps that then could be measured with gas-accepting AMS instrumentation in series. This would also facilitate increasing the number of processing standards and enable larger data-series for  $^{14}\text{C}$  quality assurance.

The results from this study demonstrate the successful use for a diversity of complex environmental matrices and the improved purification capacity of the full oxidation column that makes the recombustion of gas sample splits unnecessary. Further, the bicarbonate procedural standards now allow each operator to implement individual quality control measures.

**SUPPLEMENTARY MATERIAL**

To view supplementary material for this article, please visit <https://doi.org/10.1017/RDC.2023.13>

**ACKNOWLEDGMENTS**

The authors thank the NOSAMS staff for support of the analyses, Sean Sylva for critical discussions, Mark Roberts for help setting up the RGA interface, and Adam Subhas for support during the bicarbonate dissolution experiment. Reviews by Brad E Rosenheim and another anonymous reviewer provided valuable comments to improve the quality of this paper. We are grateful to Brad E Rosenheim and Bao Rui for sample materials, Josh Hvalenka for the technical sketch of the instrument, and Bob Nelson for helping with sampling the salt marsh sedimentary sequence in Wild Harbor, Falmouth, MA, USA. Author UMH acknowledges the NSF for funding his postdoctoral position at NOSAMS (OCE 1755125).

**REFERENCES**

- Bao R, McNichol AP, Hemingway JD, Lardie Gaylord MC, Eglinton TI. 2019. Influence of different acid treatments on the radiocarbon content spectrum of sedimentary organic matter determined by RPO/accelerator mass spectrometry. *Radiocarbon* 61(2):395–413.
- Bao RM, Strasser M, McNichol AP, Haghypour N, McIntyre C, Wefer G, Eglinton TI. 2018. Tectonically-triggered sediment and carbon export to the Hadal zone. *Nature Communications* 9(1):1–8.
- Cruz AJ, Gagnon AR, McNichol AP, Burton JR, Elder KL, Lardie GMC, Gospodinova KD, Hlavenka J, Kurz MD, Longworth BE, Roberts ML, Trowbridge NY, Walther T, Xu L. 2017. Advances in sample preparation at the National Ocean Sciences Accelerator Mass Spectrometry Facility (NOSAMS): Investigation of Carbonate Secondary Standards.
- Currie LA, Benner BA, Cachier HA, Cary R, Chow JC, Urban DL, Eglinton TI, Gustafsson O, Hartmann PC, Hedges JI, et al. 2002. A critical evaluation of interlaboratory data on total, elemental, and isotopic carbon in the carbonaceous particle reference material, NIST SRM 1649a. *Journal of Research of the National Institute of Standards and Technology* 107(3):279–298.
- Fernandez A, Santos GM, Williams EK, Pendergraft MA, Vetter L, Rosenheim BE. 2014. Blank corrections for ramped pyrolysis radiocarbon dating of sedimentary and soil organic carbon. *Analytical Chemistry* 86(24):12085–12092.
- Grant KE, Galy VV, Chadwick OA, Derry LA. 2019. Thermal oxidation of carbon in organic matter rich volcanic soils: insights into SOC age differentiation and mineral stabilization. *Biogeochemistry* 144(3):291–304.
- Haghypour N, Ausin B, Usman MO, Ishikawa N, Wacker L, Welte C, Ueda K, Eglinton TI. 2019. Compound-specific radiocarbon analysis by elemental analyzer-accelerator mass spectrometry: precision and limitations. *Analytical Chemistry* 91(3):2042–2049.
- Hanke UM, Wacker L, Haghypour N, Schmidt MWI, Eglinton TI, McIntyre CP. 2017. Comprehensive radiocarbon analysis of benzene polycarboxylic acids (BPCAs) derived from pyrogenic carbon in environmental samples. *Radiocarbon* 59(4):1103–1116.
- Hedges JI, Eglinton G, Hatcher PG, Kirchman DL, Arnosti C, Derenne S, Evershed RP, Kögel-Knabner I, De Leeuw JW, Littke R, Michaelis W, Rullkötter J. 2000. The molecularly-uncharacterized component of nonliving organic matter in natural environments. *Organic Geochemistry* 31(10):945–958.
- Hemingway JD, Galy VV, Gagnon AR, Grant KE, Rosengard SZ, Soulet G, Zigah PK, McNichol AP. 2017a. Assessing the blank carbon contribution, isotope mass balance, and kinetic isotope fractionation of the ramped pyrolysis/oxidation instrument at nosams. *Radiocarbon* 59(1):179–193.
- Hemingway JD, Hilton RG, Hovius N, Eglinton TI, Haghypour N, Wacker L, Chen MC, Galy VV. 2018. Microbial oxidation of lithospheric organic carbon in rapidly eroding tropical mountain soils. *Science* 360(6385):209–212.
- Hemingway JD, Rothman DH, Grant KE, Rosengard SZ, Eglinton TI, Derry LA, Galy VV. 2019. Mineral protection regulates long-term global preservation of natural organic carbon. *Nature* 570(7760):228–231.
- Hemingway JD, Rothman DH, Rosengard SZ, Galy VV. 2017b. Technical note: an inverse

- method to relate organic carbon reactivity to isotope composition from serial oxidation. *Biogeosciences* 14(22):5099–5114.
- NIST. 2007. Certificate of Analysis Standard Reference Material 1649a. National Institute of Standards and Technology.
- Peralta O, Baumgardner D, Raga GB. 2007. Spectrothermography of carbonaceous particles. *Journal of Atmospheric Chemistry* 57(2):153–169.
- Plante A, Beaupré SR, Robert ML, Baisden T. 2013. Distribution of radiocarbon ages in soil organic matter by thermal fractionation. *Radiocarbon* 55(2–3):1077–1083.
- Roberts ML, Elder KL, Jenkins WJ, Gagnon AR, Xu L, Hlavenka JD, Longworth BE. 2019. <sup>14</sup>C blank corrections for 25–100 µg samples at the National Ocean Sciences AMS Laboratory. *Radiocarbon* 61(5):1403–1411.
- Rogers KL, Bosman SH, Lardie-Gaylord M, McNichol A, Rosenheim BE, Montoya JP, Chanton JP. 2019. Petrocarbon evolution: ramped pyrolysis/oxidation and isotopic studies of contaminated oil sediments from the Deepwater Horizon oil spill in the Gulf of Mexico. *PLoS One* 14(2):1–21.
- Rosenheim BE, Day MB, Domack E, Schrum H, Benthien A, Hayes JM. 2008. Antarctic sediment chronology by programmed-temperature pyrolysis: methodology and data treatment. *Geochemistry, Geophysics, Geosystems* 9(4):1–16.
- Sanderman J, Grandy SA. 2020. Ramped thermal analysis for isolating biologically meaningful soil organic matter fractions with distinct residence times. *Soil* 6(1):131–144.
- Santos GM, Southon JR, Drenzek NJ, Ziolkowski LA, Druffel ERM, Xu X, Zhang D, Trumbore SE, Eglinton TI, Hughen KA. 2010. Blank assessment for ultra-small radiocarbon samples: chemical extraction and separation versus AMS. *Radiocarbon* 52(2–3):1322–1335.
- Santos GM, Southon JR, Griffin S, Beaupre SR, Druffel ERM. 2007. Ultra small-mass AMS <sup>14</sup>C sample preparation and analyses at KCCAMS/UCI facility. *Nuclear Instruments and Methods in Physics Research B* 259(1):293–302.
- Slater GF, White HK, Eglinton TI, Reddy CM. 2005. Determination of microbial carbon sources in petroleum contaminated sediments using molecular <sup>14</sup>C analysis. *Environmental Science and Technology* 39(8):2552–2558.
- Subt C, Yoon HI, Yoo KC, Lee JI, Leventer A, Domack EW, Rosenheim BE. 2017. Publications, *Geochemistry, Geophysics, Geosystems* 18: 1404–1418.
- Venturelli RA, Siegfried MR, Roush KA, Li W, Burnett J, Zook R, Fricker HA, Priscu JC, Leventer A, Rosenheim BE. 2020. Mid-Holocene grounding line retreat and readvance at Whillans Ice Stream, West Antarctica. *Geophysical Research Letters* 47(15):1–11.
- Walker BD, Xu X. 2019. An improved method for the sealed-tube zinc graphitization of microgram carbon samples and <sup>14</sup>C AMS measurement. *Nuclear Instruments and Methods in Physics Research, Section B* 438:58–65.
- White HK, Xu L, Hartmann P, Quinn JG, Reddy CM. 2013. Unresolved complex mixture (UCM) in coastal environments is derived from fossil sources. *Environmental Science and Technology* 47(2):726–731.
- White HK, Xu L, Lima ALC, Eglinton TI, Reddy CM. 2005. Abundance, composition, and vertical transport of PAHs in marsh sediments. *Environmental Science and Technology* 39(21):8273–8280.
- Xu L, Roberts ML, Elders KL, Kurz MD, McNichol AP, Reddy CM, Ward CP, Hanke UM. 2021. Radiocarbon in dissolved organic carbon by UV oxidation: procedures and blank characterization at NOSAMS. *Radiocarbon* 63(1):357–374.
- Zhang X, Bianchi TS, Cui X, Rosenheim BE, Ping CL, Hanna AJM, Kanevskiy M, Schreiner KM, Allison MA. 2017. Permafrost organic carbon mobilization from the watershed to the Colville River delta: evidence from <sup>14</sup>C ramped pyrolysis and lignin biomarkers. *Geophysical Research Letters* 44(22):11,491–11,500.
- Zigah PK, Minor EC, McNichol AP, Xu L, Werne JP. 2017. Constraining the sources and cycling of dissolved organic carbon in a large oligotrophic lake using radiocarbon analyses. *Geochimica et Cosmochimica Acta* 208(April): 102–118.